Polish J. Chem., **77**, 683–700 (2003)

Physicochemical Properties of CuAlMCM-41 and CuNbMCM-41 Mesoporous Molecular Sieves*

by I. Sobczak[1], M. Ziolek[1], I. Nowak[1], M. Daturi[2] and J.C. Lavalley[2]**

[1]*A. Mickiewicz University, Faculty of Chemistry, Grunwaldzka 6, 60-780 Poznan, Poland*
[2]*Laboratoire de Catalyse et Spectrochimie, UMR 6506 - ENSICaen - Université, 6, Boulevard du Maréchal Juin – 14050 Caen Cedex, France*

(Received October 30th, 2002)

The texture and surface properties of copper-containing aluminosilica and niobiosilica mesoporous molecular sieves of MCM-41 type, in which all elements were introduced during the synthesis, have been studied by means of XRD, N_2 adsorption, H_2-TPR, FTIR combined with pyridine and NO adsorption as well as in the skeletal region, and the test reaction. The results were compared with those obtained earlier for Cu post synthesis exchanged AlMCM-41 and NbMCM-41. All the results and this comparison allow the suggestion that copper is partially located in the skeleton of both MCM-41 materials, which exhibit redox and acidic properties.

Key words: CuAlMCM-41, CuNbMCM-41, texture, redox and acidic properties

The discovery of mesoporous molecular sieves of MCM-41 type in 1992 [1,2] opened a new possibility of heterogeneous catalysts application in the synthesis and transformation of bulky organic molecules. Many various elements have been incorporated into the skeleton of the MCM-41 material besides silicon. New elements in the molecular sieves generate new active sites. The acidity of aluminosilica (AlMCM-41) and niobiosilica (NbMCM-41) mesoporous molecular sieves has already been compared [3]. The number of surface Lewis acid sites, in the dehydroxylated hydrogen form of these materials, was higher in the case of Nb-containing sample, but the strength of these centres was lower on NbMCM-41 in comparison with that on AlMCM-41 matrix.

The redox properties have been generated in the mesoporous molecular sieves *via* the introduction of various transition or early transition metals. Among others, copper [4–13], iron [14–18], vanadium [19–20], and niobium [3,21–23] containing MCM-41 were studied. Transition metal can occupy the extra framework site or can be incorporated into the skeleton of the material. Depending on that, various active centres are formed. Many redox catalytic processes involve the presence of both redox and acidic centres (*e.g.* selective catalytic reduction of NO with hydrocarbons – HC-SCR [24–26] or the oxidation (hydroxylation) of organic compounds, which

* Dedicated to the memory of Professor Stanisław Malinowski in appreciation of his outstanding contributions to acid-base catalysis.

** Corresponding author: Tel: (+4861) 8291243, e-mail: ziolek@amu.edu.pl

requires the ring opening step [27–28]. Therefore, the preparation of bifunctional catalysts is important. This paper is located in this range of studies. Our goal was to obtain the bifunctional catalysts *via* the incorporation of two various elements (besides silicon) into MCM-41 mesoporous sieves, thus, we prepared the materials containing CuAlSi and CuNbSi in the mesoporous molecular sieve framework. The aim of this study was the characterization of texture and structure properties of these materials as well as the estimation of their acidic properties.

EXPERIMENTAL

Catalyst preparation: Novel synthesis at room temperature (adapted from paper of Unger *et al*. [29]) of CuAlMCM-41-32 (32 means Si/T ratio, T = Cu + Al) was done in the following way: ethanol (98-vol.%, 50 cm^3; POLMOS-Poland) and aqueous ammonia (32-wt.%, 15.4 cm^3; POCH-Poland) were added to the surfactant solution – cetyltrimethylammonium (CTA) chloride in water (52 g, 25-wt.% in water; ALDRICH). The solution was stirred for 10 min and tetraethoxysilane – TEOS (98 wt.%, 3.4 g; ALDRICH) was added followed by aluminium sulfate (0.085 g dissolved in 5 g of water, POCH-Poland) and copper(II) acetate (0.050 g in 6 g of water, POCH-Poland) solutions. After stirring for 2 h at room temperature the resulting precipitate was recovered by filtration, washed with distilled water and dried in air at room temperature. The template was removed by calcination at 823 K for 8 h.

The synthesis of CuNbMCM-41-32 (32 means Si/T ratio, T = Cu + Nb) was performed in the same manner, but instead of aluminum sulfate niobium oxalate, as a source of niobium, was applied.

Content of Cu was estimated basing on AAS analyses of dissolved samples.

Because Si/T ratio for as prepared materials was always 32, in the following text the last number (32) in the molecular sieves symbols will be omitted.

Hydrogen forms of CuAlMCM-41-32 and CuNbMCM-41-32 materials were obtained *via* cation exchange with NH_4^+ ions and calcination of the modified samples at 723 K. The ion exchange was performed using a conventional method, *i.e.* stirring of the solid in aqueous solution of NH_4Cl (0.25 M).

N_2 adsorption/desorption: The surface area and pore volume of the MCM-41 materials were measured by nitrogen adsorption at 77 K using the conventional technique on a Micromeritics 2010 apparatus.

X-ray diffraction: The XRD patterns were obtained on a TUR-62 diffractometer using CuK_α radiation.

FTIR measurements in the skeletal region: Infrared studies were performed on a Vector 22 (Brucker) FTIR spectrometer in the skeletal region (1500–400 cm^{-1}) using pellets containing 1 mg of the sample and 200 mg of Kbr.

H_2-TPR measurements: The temperature-programmed reduction (TPR) of the samples was carried out using H_2/Ar (10 vol.%) as reducing agent (flow rate = 32 cm^3 min^{-1}). The sample (0.03 g) was filled in a quartz tube, treated in a flow of helium at 723 K for 1 h and cooled to room temperature. Then it was heated at a rate of 10 K min^{-1} to 1300 K under the reducing mixture. Hydrogen consumption was measured by a thermal conductivity detector in the PulseChemiSorb 2705 (Micromeritics) apparatus.

FTIR measurements in vacuum cell: FTIR spectroscopy was used for characterization of Cu species in the catalysts and complexes formed after NO adsorption and decomposition. Infrared spectra were recorded with a Nicolet Magna 550 FTIR spectrometer using a quartz in situ cell. The samples were pressed under low pressure into wafers of ~ 5 mg cm^{-2} and placed in the cell. The catalysts were activated in the following conditions: calcination under pure O_2 at 723 K for 1 hour, cooling to room temperature (RT), evacuation of oxygen at RT, evacuation at 723 K for 7 hours. The experiments were carried out in two ways: i) NO adsorption at RT, ii) NO adsorption followed by evacuation at RT during 15 min, then heating to 673 K. All spectra were recorded at room temperature.

Pyridine adsorption on the catalysts was conducted after the activation protocol described above. After saturation with pyridine the samples were degassed at RT, 423, 523, 623 and 723 K in high vacuum for 30 min.

Catalytic test: The acid characteristics of the catalysts were evaluated using acetonylacetone (AcAc) cyclization as probe reaction – [30,31]. In this reaction dimethylfuran (DMF) is produced on acidic centres, whereas basic centres are involved in the formation of methylcyclopentenone (MCP).

The catalyst bed (0.05 g) was first activated for 2 hours at 723 K under nitrogen flow. The reaction was conducted in a pulse-flow micro-reactor in which 0.6 cm^3 of AcAc was passed continuously over the catalyst at 523 K in a nitrogen stream. The reaction products were collected downstream of the reactor in a cold trap and analysed by gas chromatography (CHROM -5, Silicone SE-30/Chromosorb column).

RESULTS AND DISCUSSION

Composition: The composition of the catalysts, shown in Table 1, indicates that a lower number of copper atoms are included into niobiosilica than aluminosilica matrix. Stirring of aqueous suspensions of the samples at room temperature or the NH_4^+ exchange procedure lead to the partial removal of copper documented by the increase of Si/Cu ratio. This increase is much higher in the case of CuAlMCM-41 than CuNbMCM-41. It is worthy of notice that after the removal of less held copper in both materials (caused by stirring of aqueous suspensions) the Cu/Al and Cu/Nb ratios are almost the same (0.54 and 0.53, respectively). It suggests that for the incorporation of copper into the framework the ratio of Cu:Al(Nb) should not be higher than 1:2.

Table 1. Composition of the CuAl(Nb)MCM-41 catalysts.

Catalyst	Si/Al(Nb) as assumed	Si/Cu	Cu/Al(Nb)
CuAlMCM-41-32	64	98	0.65
CuAlMCM-41-32 w	64	118	0.54
H-CuAlMCM-41-32	64	112	0.57
CuNbMCM-41-32	64	114	0.56
CuNbMCM-41-32 w	64	120	0.53
H-CuNbMCM-41-32	64	118	0.54

w – catalyst after stirring in water at room temperature for 8 hours.

N_2 adsorption/desorption measurements: The textural properties of the prepared samples are summarized in Table 2. The comparison of the data for monometallic (Al and Nb) and bimetallic (CuAl and CuNb) materials does not show significant differences caused by the incorporation of copper. However, a slight decrease of surface area and pore volume as well as the increase of average pore diameter is clearly seen. It is also true for external surface areas and mesopores surface areas as well as for mesopores pore volume – all calculated from t-plot. This behaviour suggests the incorporation of Cu into the framework. One should remember that mesoporous molecular sieves prepared according to the so called "fast synthesis" exhibit higher surface area and lower pore volume and pore diameter [32] than the materials synthesized using the hydrothermal method [1,2].

Table 2. Textural properties of mesoporous molecular sieves calculated from N_2 ads./des. isotherms and t-plots.

Catalyst	Surface area, m^2/g				Pore volume, cm^3/g		Average pore diameter, nm
	BET	BJH des.	external*	meso*	BJH des.	meso*	
AlMCM-41-32	1183	1587	56	1189	1.163	0.899	2.9
NbMCM-41-32	1153	1451	42	1268	0.999	0.780	2.8
CuAlMCM-41-32	1111	1476	47	1080	1.044	0.787	3.2
CuNbMCM-41-32	1114	1446	31	1131	0.939	0.734	2.8
CuAlMCM-41-32 w	1149	1407	47	1187	0.978	0.786	2.8
CuNbMCM-41-32 w	1107	1365	32	1165	0.902	0.675	2.6

* – calculated from t-plot.
w – catalyst after stirring in water at room temperature for 8 hours.

N_2 adsorption/desorption isotherms for both investigated samples (Fig. 1) are typical of mesoporous materials (type IV of isotherms according to IUPAC classification). They exhibit a sharp inflection at a relative pressure of about 0.3, characteristic of capillary condensation in uniform mesopores. Almost no hysteresis loop was detected in this region, which proves a high quality mesoporous framework. The BJH pore distribution (Fig. 1) indicates a narrow and monomodal pore size distribution centred at *ca*. 2.5–2.8 nm. There was no macroporosity observed in both samples.

The stirring of the CuMCM-41 materials in water does not change significantly the texture and structure properties of the materials. The data in Table 2 point to slight decrease of surface area, pore volume and pore diameter after treatment with water.

X-ray diffraction study: XRD patterns of both samples (CuAlMCM-41 and CuNbMCM-41) are shown in Fig. 2. They exhibit one distinctive peak at $2\Theta = 2.5°$ indexed as [100]. The other three peaks between 3–6° are not well resolved and overlap each other. It indicates that the material is not well ordered. Nevertheless, the presented patterns are typical of hexagonal arranged mesoporous materials of MCM-41 type [2].

XRD pattern of CuNbMCM-41 in the high angle range exhibits a broad peak ($2\Theta \approx 13°$) indicating the presence of an additional phase besides that of mesoporous tubes. This new phase is stable even after 8 hours stirring of the material with water. Such a treatment causes the distortion of the mesopores ordering as indicated by the diminishing of XRD peaks in the 3–6° range. CuAlMCM-41 molecular sieve shows a small reflex at $2\Theta \approx 32°$, which can be assigned to some kind of copper-oxygen crystal phase (CuO gives rise to peak at $2\Theta \approx 35{,}7°$ [37,38]) or another phase formed as a result of copper-alumina or copper-silica interaction. The phase described by the XRD peak at $2\Theta \approx 13°$ (observed in CuNbMCM-41) appears on CuAlMCM-41 after 6 months exposition to air and after stirring in water. The latter treatment does not cause the diminishing of XRD peaks at 3–6° range characterizing the hexagonal ordered of mesopores.

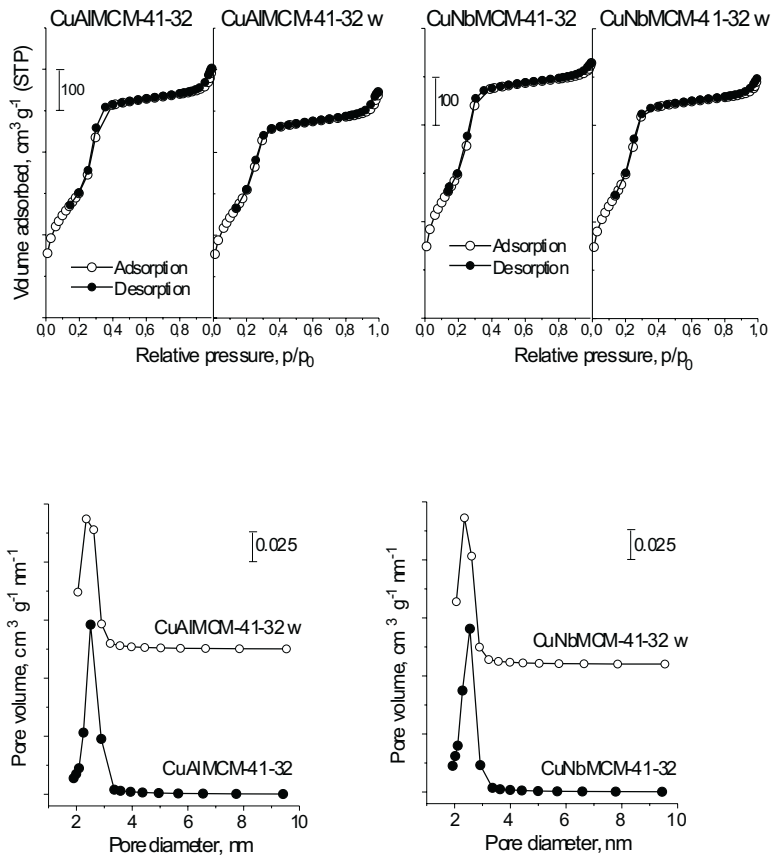

Figure 1. N_2 adsorption/desorption isotherms and pore size distribution of CuMCM-41 materials. w – catalyst after stirring in water.

FTIR study in the skeletal range: Fig. 3 presents the infrared spectra of CuAlMCM-41 and CuNbMCM-41 samples. They are typical of siliceous mesoporous MCM-41 materials containing heteroatoms other than Si as shown by the well visible band at about 965 cm^{-1}. This band is interpreted in the literature [33–35] as the effect of the distortion of skeletal Si–O–Si vibrations caused by the presence of metal cations in the framework or extra framework positions. Thus, the presence of ~965 cm^{-1} IR band cannot be used as a proof for the incorporation of metal into the siliceous skeleton.

H_2-TPR study: In order to analyse the reducibility of metal species in CuAlMCM-41 and CuNbMCM-41 the temperature-programmed reduction (H_2-TPR) of the samples was performed. Fig. 4 displays the H_2-TPR profiles of the starting catalysts as well as the materials stirred in water. For comparison, the reduction of CuO activated at various temperatures is exhibited. At the temperature below 700 K the

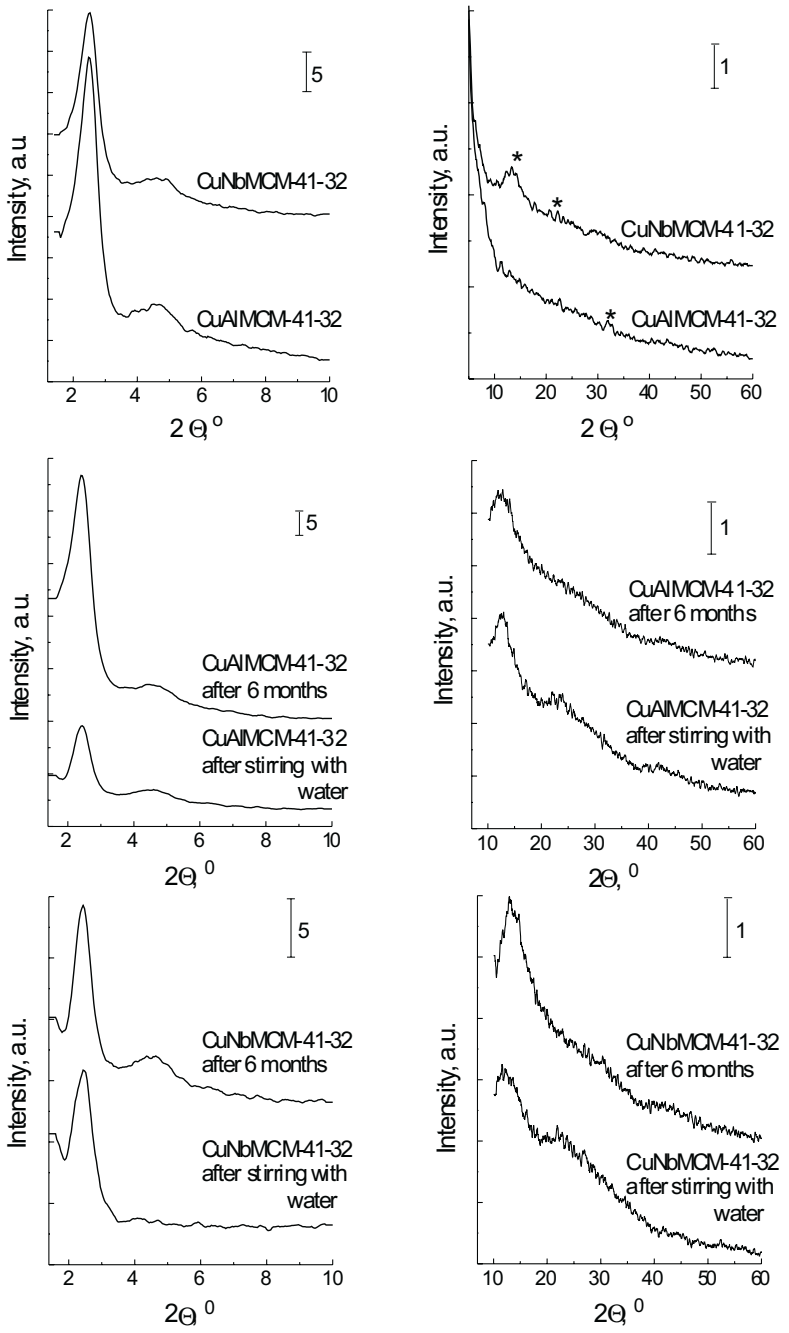

Figure 2. XRD patterns of CuMCM-41 molecular sieves.

H_2-TPR peaks origin from copper reduction. There is an agreement in the literature [36–40] for the following assignment of the H_2-TPR peaks:

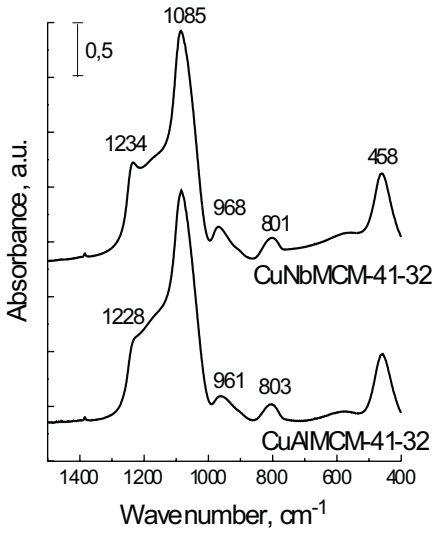

Figure 3. FTIR spectra of CuMCM-41 in the skeletal range.

$CuO + H_2 \rightarrow Cu^0 + H_2O$ (H_2-TPR peak in the 440–480 K range) (1)

isolated $Cu^{2+} + 1/2\ H_2 \rightarrow Cu^+ + H^+$ (> 480 K) (2)

$Cu^+ + 1/2\ H_2 \rightarrow Cu^0 + H^+$ (> 600 K) (3)

As shown in Fig. 4, CuO activated at 723 K is partially reduced and therefore gives rise to the reduction peak at a higher temperature, but below 600 K.

The H_2-TPR profiles of CuAlMCM-41 and CuNbMCM-41 indicate the reduction of copper species at 583 K in the case of Al neighbour and at 560 K in CuNbMCM-41 sample. One should assign it to the reduction of isolated Cu^{2+} to Cu^+. There is no evidence from H_2-TPR profiles for further reduction of Cu^+, which should occur at temperature above 600 K. A shoulder at ~536 K may be due to the reduction of copper-oxygen phase (not necessary CuO).

In the high temperature range (> 1050 K) the H_2-TPR peaks (CuNbMCM-41) due to the reduction of niobium located in the skeleton can be observed [7,8,23]. Interestingly, the stirring of aqueous suspension of this sample causes not only the removal of copper from the extra framework position (no peaks due to copper reduction), but also the removal of niobium from the framework or rather the opening to the view of niobium surface species (Fig. 4). Copper is leached by water, whereas niobium is located in the extra framework position strongly held onto the surface of the molecular sieve or on the internal surface of walls. This statement bases on the H_2-TPR (Fig. 4, CuNbMCM-41, b) profile typical of the material obtained *via* niobium impregnation

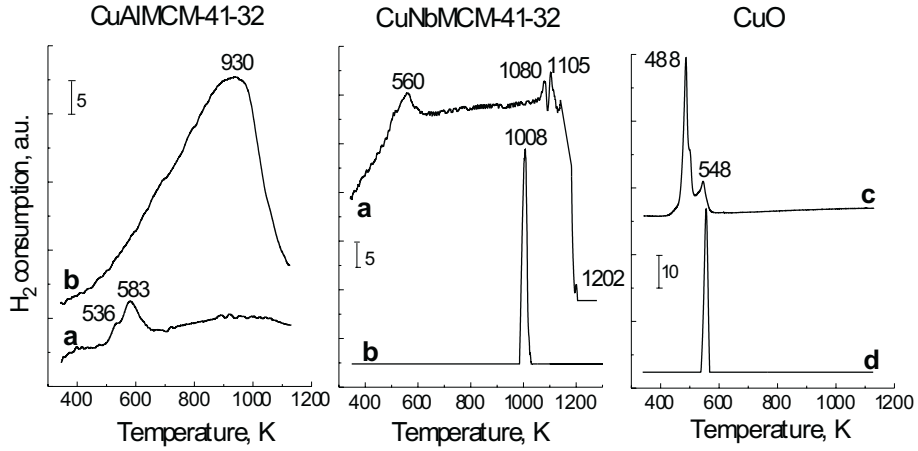

Figure 4. H_2-TPR profiles of CuMCM-41: fresh sample (a), sample after stirring in water (b); and CuO: activated at 393 K (c), 723 K (d).

of siliceous MCM-41 [23]. Water treatment also causes the removal of copper species from CuAlMCM-41, as evidenced by the disappearance of Cu-reduction peaks in the H_2-TPR profile (Fig. 4).

The localization of Cu species, which are reduced with hydrogen, can be estimated on the basis of sulphate formation upon the interaction with $SO_2 + O_2$ mixture. The H_2-TPR profiles of two copper aluminosilica samples, prepared by using various methods and sulphated with $SO_2 + O_2$ at 673 K, are displayed in Fig. 5. CuAlMCM-41 material was prepared according to the procedure described in this paper, whereas Cu-AlMCM-41-32-132 was obtained *via* Cu^{2+} cation exchange in AlMCM-41-32 molecular sieve. In the first material we expect to incorporate copper into the skeleton together with Al and Si, while in the second, copper is located in the extra framework position. The similarity of H_2-TPR profiles for both samples suggests that in both materials the same Cu-species and Cu-sulphate species are reduced by hydrogen. 580–586 K peaks can be due to the reduction of Cu^{2+} ions connected with the framework or sulphate ions, and the peak at 615 K and 630 K origins from the reduction of copper-sulphate species. On this basis one can suppose that in CuAlMCM-41 sample a part of copper occupies the extra framework position.

Hydroxyl groups: Infrared spectra in the ν(OH) region, recorded after activation of the parent materials under vacuum and spectra of the samples prepared *via* NH_4^+ exchange, are shown in Fig. 6. All the materials exhibit a sharp band at 3745 cm^{-1} corresponding to silanol groups, very similar to that observed for SiMCM-41 [3]. The width at half height of the IR band, recorded for CuAlMCM-41 and CuNbMCM-41, is 20 cm^{-1}. After NH_4^+ exchange and deamonation the intensity of the band at 3745 cm^{-1} decreases, but the band becomes broader (half width is 30 cm^{-1} instead of 20 cm^{-1} for CuAlMCM-41 and 40 cm^{-1} instead of 20 cm^{-1} for CuNbMCM-41). A similar effect is observed when copper exchange procedure in AlMCM-41 and NbMCM-41 materials was performed (Fig. 6 a, d). Moreover, a tail towards lower wavenumbers

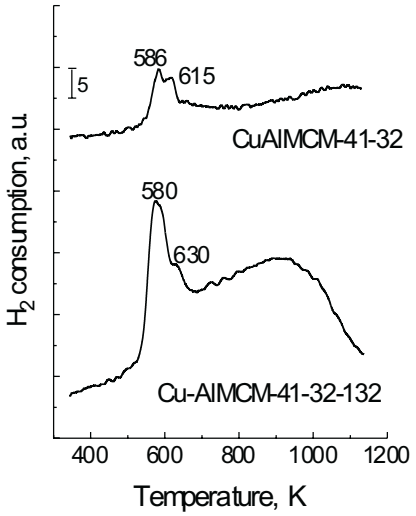

Figure 5. The effect of sulfation at 673 K on H_2-TPR profiles of CuAlMCM-41-32 and Cu-AlMCM-41-32-132.

exists in IR spectra of all samples (see Fig. 6 B). It is more pronounced for NH_4^+ exchanged materials. The discussed tail covers the bands of acidic OH groups, which will be proved below in the part describing the effect of pyridine adsorption. The fact that the tail is bigger and extended towards lower wavenumbers for H-CuAlMCM-41 and H-CuNbMCM-41 as compared with the parent materials indicates the cation exchanged properties of the molecular sieves studied.

Although Corma *et al*. [41] and Chen *et al.* [42] explained the presence of the tail in the low wavenumber range of the IR spectra as due to the interaction of silanol groups with the template, in the case of the spectra presented in this paper such an interpretation cannot be adapted. The materials used in this study were calcined in the vacuum cell before the infrared study. It allows the completely removal of the residual template. Therefore, the discussed tail cannot origin from the interaction of silanol groups with template molecules. Additional proofs for that can be found in our earlier paper [3].

The infrared spectra shown in Fig. 6 B exhibit also another tail towards higher (> 3750 cm^{-1}) wavenumbers. One can even observe a broad band at about 3850 cm^{-1} on this tail. It is noteworthy that this band is registered for all the samples, even if it is more pronounced for the molecular sieves in which copper was introduced during the synthesis (CuAlMCM-41 and CuNbMCM-41), due to the different shape of the background baseline. This band has been assigned to the ν(OH) + ν(OH) combination, *i.e*. the combination between the silanol stretching and the out-of-plane deformation corresponding to the third vibrational degree of freedom of the proton in the silanol group [43].

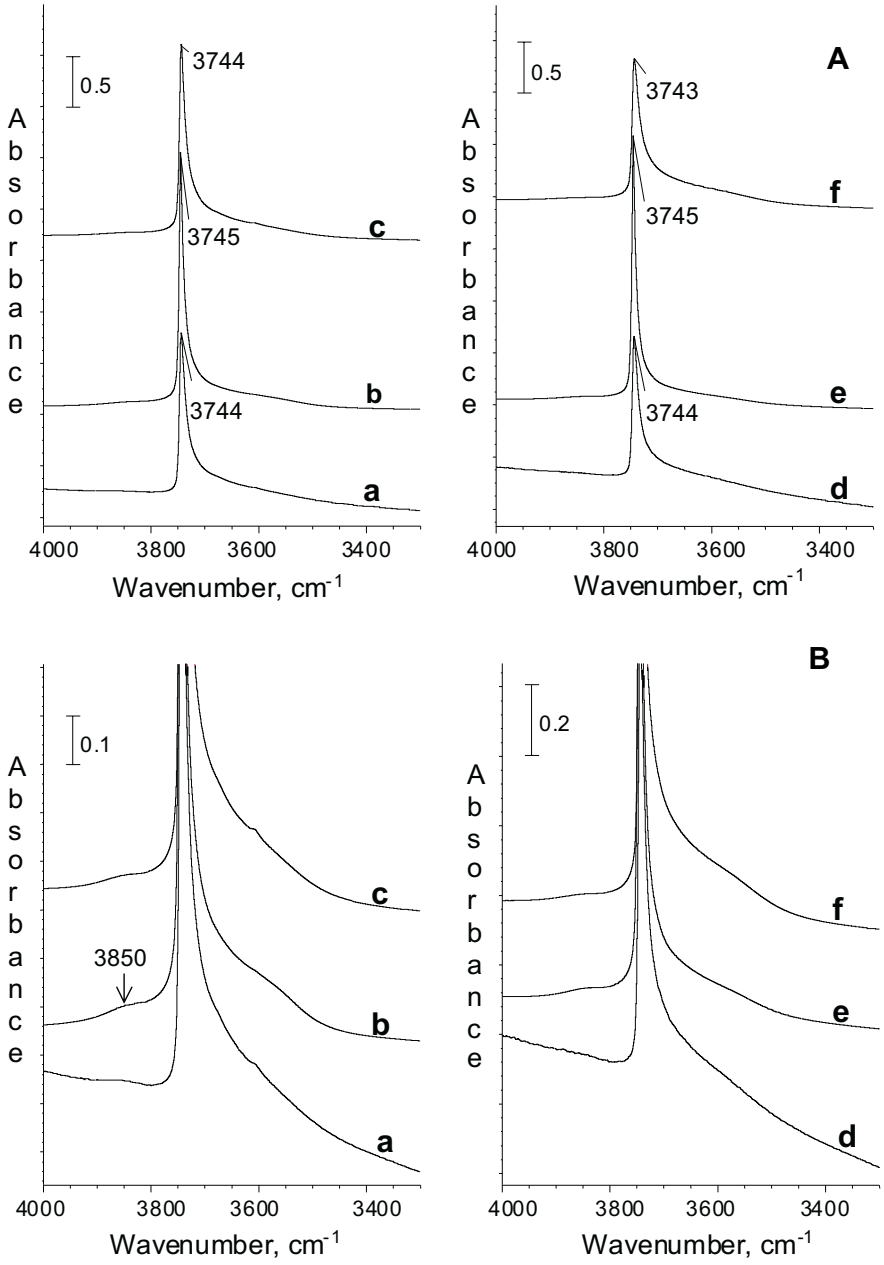

Figure 6. ν(OH) stretching region of Cu-AlMCM-41-32-132 (a), CuAlMCM-41-32 (b), H-CuAlMCM-41-32 (c), Cu-NbMCM-41-32-112 (d), CuNbMCM-41-32 (e), and H-CuNbMCM-41-32 (f), samples after activation. Spectra B are zoom of spectra represented in A.

Acidity measurements – *FTIR study*: In order to evaluate the amount and type of acidic centres, infrared spectroscopy (FTIR) measurement of adsorbed pyridine and nitrogen oxide has been applied.

Pyridine ($pK_b = 8.8$) interacts with both Brönsted (BAS) and Lewis (LAS) acid sites. Chemisorption on LAS gives rise to characteristic IR bands at ~1610 (ν_{8a}) and ~1450 (ν_{19b}) cm^{-1}. The wavenumber of the ν_{8a} bands gives information about the strength of LAS and the intensity of the ν_{19b} band is related to the number of LAS taking into account that $\varepsilon_{1450} \approx 1.5\ \mu mol^{-1}cm$ [44]. The interaction of pyridine with BAS results in the appearance of a band near 1550 cm^{-1}, which is accompanied by two others near 1640–1620 cm^{-1}. ε_{1450} has been estimated at $1.5\ \mu mol^{-1}cm$ [44].

Nitrogen(II) oxide is chemisorbed on Lewis acid sites. Depending on the value of positive charge of LAS the adsorption of NO gives rise to the IR bands of various wavelengths in the range near 1900–1700 cm^{-1}.

The interaction of NO with metal-oxide species results in the appearance of IR bands near 1600 cm^{-1}. Nitrogen oxide interacts also with Brönsted acid sites and in the presence of oxygen the following reaction occurs [45]:

$$2NO + 1/2O_2 + 2O_L\text{-}H^+ \rightarrow 2O_L\text{-}NO^+ + H_2O \quad (4)$$

L – oxygen localized in skeleton NO^+ species, is observed in the IR spectra as a band at 2133 cm^{-1}.

Pyridine (Py) adsorption: Figure 7 displays FTIR spectra of pyridine adsorbed on all samples studied and evacuated at room temperature (RT) – spectra (a), and at 423 K – spectra (b). After pyridine adsorption and desorption at room temperature on both parent materials, *i.e*. CuAlMCM-41 (Fig. 7 A) and CuNbMCM-41 (Fig. 7 C), the spectra exhibit main bands at 1624 (1627), 1611 (1610), 1597, 1579, 1490 (1488), 1446 cm^{-1} and a weak band at ~1555 cm^{-1}. The band at 1597 cm^{-1} origins from physisorbed pyridine and disappears after evacuation at 423 K (spectra b), whereas the other bands remain in the spectra of samples evacuated at 423 K, but their intensity is much lower. Both materials exhibit well defined bands at 1612 cm^{-1} characteristic of pyridine bound to Lewis acid sites (Fig. 7 A and C, spectra b). From the intensity of the PyL species at 1451 cm^{-1} (assuming that at the present evacuation temperature no hydrogen bond remains on the surface) one could estimate the number of Lewis acid sites at 455×10^{17} sites g^{-1} for CuAlMCM-41 and 167×10^{17} sites g^{-1} for CuNbMCM-41 (Table 3). The comparison of the latter number with that measured earlier for NbMCM-41-32 without copper [3] indicates that the introduction of Cu lowers the number of Lewis acid sites of the appropriate strength (which hold Py after evacuation at 423 K).

Brönsted acid sites are characterized by a PyH^+ vibration recorded at ~1550 cm^{-1}, which almost disappeared on CuNbMCM-41 after evacuation at 423 K showing that the strength of BAS is not very high. This band was more pronounced on CuAlMCM-41.

The same experiments, performed on the ammonium exchanged H-CuAlMCM-41 sample, evidenced the presence of two kinds of Lewis acid sites characterized by pairs of bands: 1447, 1612 cm^{-1} and 1451, 1624 cm^{-1} (Fig. 7B, spectrum a). It is worthy of note that two IR bands at 1444 and 1455 cm^{-1} were also registered earlier on

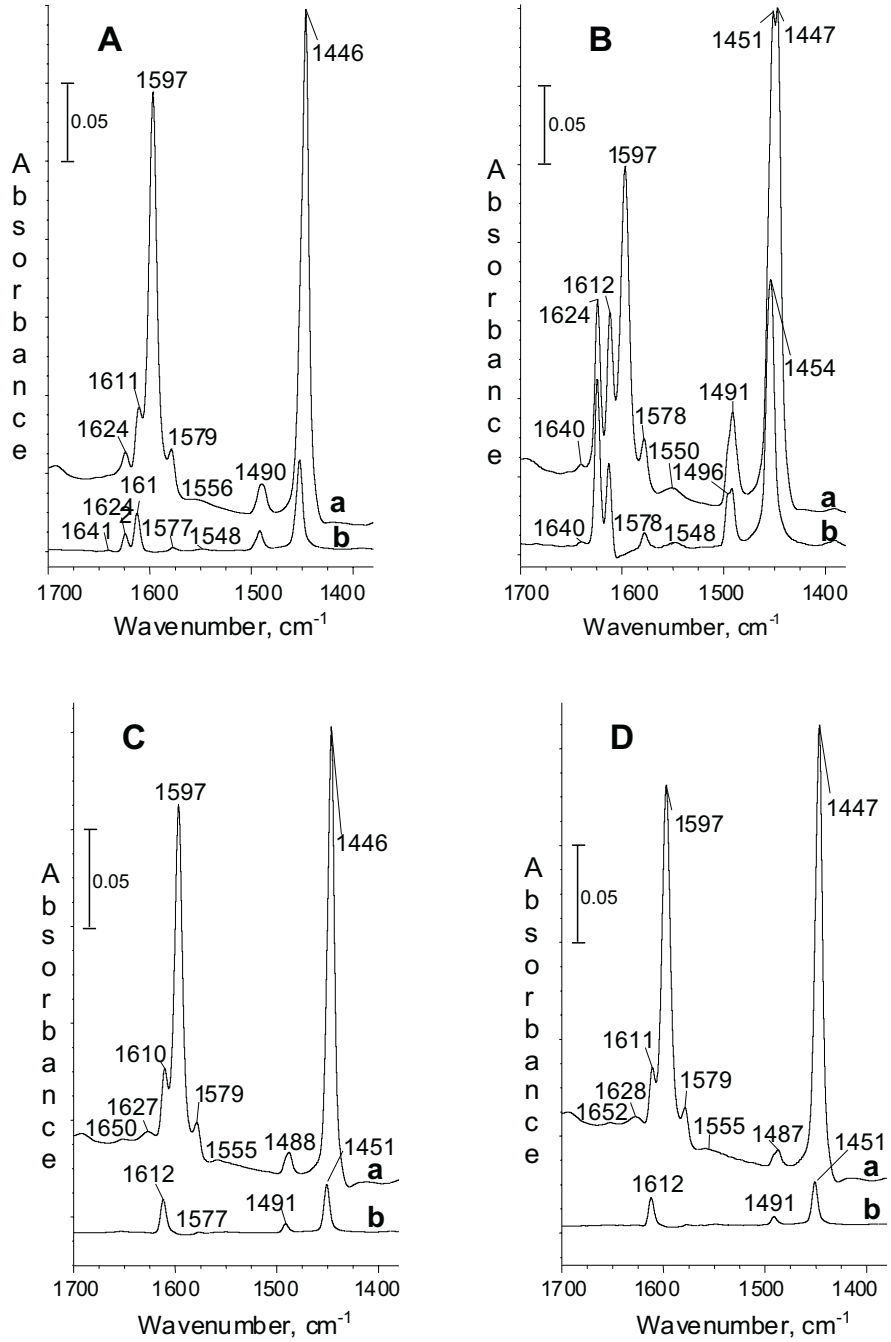

Figure 7. Pyridine adsorption after activation, then desorption at RT (a) and 423 K (b) on CuAlMCM-41-32 – A, H-CuAlMCM-41-32 – B, CuNbMCM-41-32 – C and H-CuNbMCM-41-32 – D.

H-AlMCM-41 [3] and therefore, cannot be interpreted as due to copper and aluminum species. However, copper containing H-CuAlMCM-41 material indicates much higher LAS strength than H-AlMCM-41 sample and the number of LAS after evacu-

ation at 423 K is extremely high (1857×10^{17} sites g^{-1}). Pyridine adsorption on H-CuAlMCM-41 also clearly evidences the formation of PyH^+ species (the band at 1550 cm^{-1} – Fig. 7 B, spectrum a) as a result of the interaction with Brönsted acid sites. The same species is also visible on H-CuNbMCM-41 (Fig. 7 D, spectrum a) but it almost disappears after evacuation at 423 K. The PyH^+ species on H-CuAlMCM-41 persists after evacuation at 423 K showing that the strength of Brönsted acid sites is higher on aluminum than on the niobium containing sample. The density of BAS on H-CuAlMCM-41 is much higher than on all other samples since it could be estimated at 40×10^{17} sites g^{-1}.

Table 3. Number of Brönsted acid sites (BAS) and Lewis acid sites (LAS) calculated per 1 g of the catalysts on the basis of IR bands observed after desorption of pyridine at 423 K and extinction coefficient of pyridine (LAS $\varepsilon_{1450} \approx 1.5\,\mu mol^{-1}$ cm, BAS $\varepsilon_{1550} \approx 1.8\,\mu mol^{-1}$ cm).

Catalyst	Number of LAS$\times10^{17}$	Number of BAS$\times10^{17}$	Total number of acid sites $\times10^{17}$	Ref.
Nb-MCM-41-32	208	–	208	3
HNb-MCM-41-32	523	7	529	3
CuAlMCM-41-32	455	8	463	this work
CuNbMCM-41-32	167	3	170	this work
H-CuAlMCM-41-32	1857	40	1897	this work
H-CuNbMCM-41-32	189	5	194	this work

NO adsorption: NO adsorption followed by FTIR spectroscopy characterizes Cu and Nb species. Fig. 8 displays spectra recorded on CuAlMCM-41 after the adsorption of increasing amounts of NO (part A) and heating at 573 K (part B, spectrum b), and moreover, the spectra, showed in earlier paper [9], obtained after NO adsorption on Cu-AlMCM-41-32-132 and heating at 573 K (part C). NO adsorption at room temperature (RT) on both samples leads to the formation of two fundamental bands at 1891 (1894) cm^{-1} ($Cu^{2+}NO$) and 1809 cm^{-1} ($Cu^{+}NO$). The third one at 1875 cm^{-1} is due to the presence of NO in the gas phase. However, the intensity of these bands on CuAlMCM-41 is much lower than that on Cu-exchanged material. It indicates a lower concentration of Cu-species able to interact with NO in the sample synthesized with Cu-source. This could be a reason why $Cu^{2+}O^{-}$ species characterized by the formation of a complex $Cu^{2+}O^{-}NO$ (1609 cm^{-1}) is not formed on CuAlMCM-41. There are two possibilities to explain this difference in copper detection for the two samples: i) Cu, which interacts with NO, is located in the extra framework sites and the other in the framework of CuAlMCM-41; ii) all Cu is located in the framework of CuAlMCM-41, but a part of copper is inside the walls of mesoporous sieves and is not accessible for NO molecules.

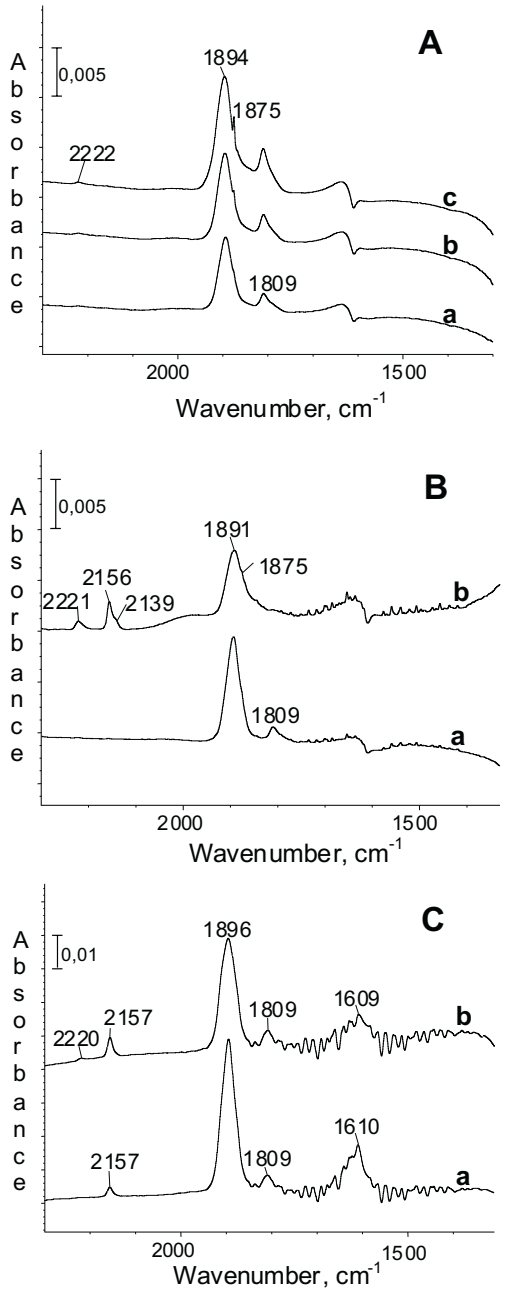

Figure 8. FTIR subtracted spectra of copper modified AlMCM-41 after the following operations:
A – CuAlMCM-41-32: NO adsorption at RT a) 0.25 mmol g^{-1}, b) 0.75 mmol g^{-1}, c) full saturated sample;
B – CuAlMCM-41-32: a) NO adsorption at RT, 0.5 mmol g^{-1}, followed by evacuation at RT, 15 min, b) heating at 573 K, 30 min;
C – Cu-AlMCM-41-32-132: a) NO adsorption at RT, 0.5 mmol g^{-1}, followed by evacuation at RT, 15 min, b) heating at 573 K, 30 min.

Heating of CuAlMCM-41 in the presence of the adsorbed nitrogen oxide (Fig. 8 B) causes the transformation of NO to N_2O (2221 cm^{-1}) and NO^+ species (~2139 cm^{-1}). N_2O is formed in the reaction:

$$2NO \rightarrow N_2O + 1/2O_2 \quad (5)$$

Oxygen takes part in the reaction between H^+ and NO according to the equation (4) and gives rise to NO^+ generation. A band at 2156 cm^{-1} could be assigned to CO formed as a result of the residual template oxidation with O_2 coming from the reaction (5). The other possibility is the origin of this band from NO^+ located on the different site [46] or NO_2^+ [47].

The same experiment performed on CuNbMCM-41 led to similar results (Fig. 9). NO chemisorbed on this material exhibits the bands at ~1889 cm^{-1} ($Cu^{2+}NO$), ~1782 cm^{-1} ($Cu^{\delta+}NO$, $\delta < 1$) and ~1606 cm^{-1} (most probably from the complex $\geqslant NbO^-NO$).

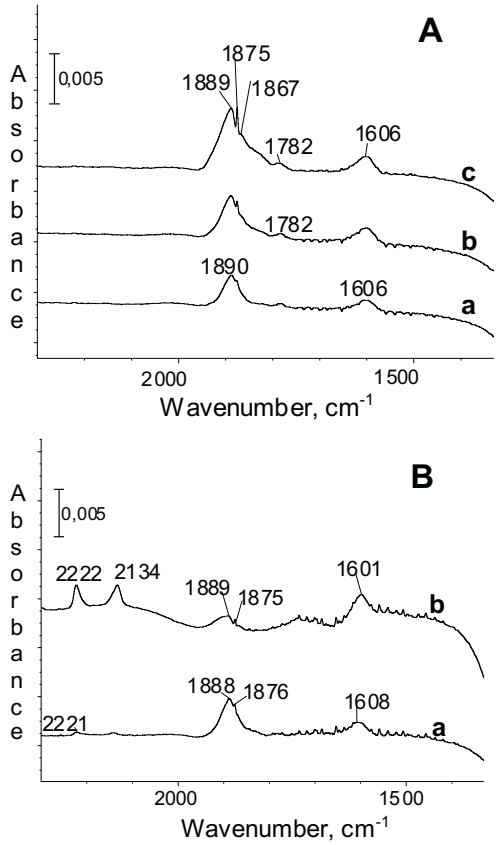

Figure 9. FTIR subtracted spectra of copper modified NbMCM-41 after the following operations:
A– CuNbMCM-41-32: NO adsorption at RT a) 0.25 mmol g^{-1}, b) 0.75 mmol g^{-1}, c) full saturated sample;
B– CuNbMCM-41-32: a) NO adsorption at RT, 0.5 mmol g^{-1}, followed by evacuation at RT, 15 min, b) heating at 573 K, 30 min.

The heating of chemisorbed NO gives rise to N_2O and NO^+ appearance. There is not a band at 2157 cm^{-1}.

The FTIR study of NO adsorbed clearly shows that both materials (CuAlMCM-41 and CuNbMCM-41) exhibit redox properties as evidenced from the reaction (5) and confirms the presence of active protons (Brönsted acid sites).

Catalytic experiments: *Acidity* of the investigated catalysts has been confirmed by the results of the acetonylacetone (AcAc) decomposition [30,31] presented in Table 4.

Table 4. Results of the catalytic test reaction on CuAl(Nb)MCM-41 catalysts.

Catalyst	AcAc conversion, %	DMF selectivity, %
CuAlMCM-41-32	11.5	100
H-CuAlMCM-41-32	34.8	100
CuNbMCM-41-32	2.4	100
H-CuNbMCM-41-32	5.8	100

Dimethylfuran (DMF) formation, in the absence of the bases catalysed product – methylcyclopentenone (MCP) – confirms the acidic character of both materials, CuAlMCM-41 and CuNbMCM-41. The acidity evidently increases for hydrogen forms of the materials, as the DMF product is formed on Brönsted acid sites. Lewis acid centres are not involved in DMF formation. The highest AcAc conversion to DMF on H-CuAlMCM-41 corresponds to the higher number of Brönsted acid sites shown in Table 3. The activity of all the samples in AcAc conversion well correlates with the number of BAS calculates from FTIR spectra.

CONCLUSIONS

The prepared samples exhibit hexagonal arrangement of mesopores typical of MCM-41 molecular sieves with uniform narrow pore size distribution and an additional, non identified, phase. They were stable for 6 months exposition to air but less stable during long term stirring in water. The latter leads to the partial removal of Cu and Nb from mesoporous sieves. Removed Nb is located in the extra framework position or on the internal surface of walls, whereas Cu is leached to the solution. However, the chemical analyses of the materials stirred in water indicate only slightly decrease of the amount of copper (the increase of Si/Cu ratio – Table 1). One can postulate that only copper located in the extra framework position is leached and that incorporated into the skeleton is stable. Thus, copper in the framework is not reduced by hydrogen and therefore the samples stirred in water do not exhibit H_2-TPR peaks originating from copper reduction (Fig. 4). Moreover, Cu located in the framework seems does not interact with $SO_2 + O_2$ mixture forming Cu-sulphate species, which can be reduced by hydrogen, because H_2-TPR profile exhibits only reduction of Cu (extra framework) – sulphate species.

There is no direct proof for the incorporation of Cu into the skeleton of mesoporous molecular sieves. However, there are some indirect suggestions of that. The decrease of the pore volume of Cu-containing samples (Table 2) in comparison with the aluminosilica and niobiosilica materials suggests the incorporation of new element (Cu) into the framework. Moreover, the fact that after stirring the samples in water still Cu is left in the material allow us to suppose that copper is located in the skeleton.

Both, CuAlMCM-41 and CuNbMCM-41, mesoporous molecular sieves exhibit redox properties and present small amount of Brönsted acid sites (concluded on the basis of FTIR study combined with PY and NO adsorption and the test reaction). This fact seems to be promising for a further application of these materials in the oxidation processes requiring the presence of a low number of Brönsted acid sites accompanying the redox centres.

Acknowledgments

This work was partially supported by the Polish State Committee for Scientific Research (KBN Grant No 3T09A 102 19). I Sobczak would like to thank for the grant from Fundation for Polish Science.

REFERENCES

1. Kresge C.T., Leonowicz M.E., Roth W.J., Vartuli J.C. and Beck J.S., *Nature*, **359**, 710 (1992).
2. Beck J.S., Vartuli J.C., Roth W.J., Leonowicz M.E., Kresge D.T., Schmitt K.D., Chu C.T.W., Olson D.H., Sheppard E.W., McCullen S.B., Higgins J.B. and Schlenker J.L*., J. Am. Chem. Soc*., **114**, 1083 (1992).
3. Ziolek M., Nowak I. and Lavalley J.C., *Catal. Lett*., **45**, 259 (1997).
4. Ziolek M., Sobczak I., Decyk P. and Nowak I., *Polish J. Environmental Studies*, **6**, 47 (1997).
5. Ziolek M, Sobczak I., Decyk P. and Nowak I., *Stud. Surf. Sci. Catal*., **125**, 633 (1999).
6. Ziolek M., Nowak I., Sobczak I., Lewandowska A., Decyk P. and Kujawa J., *ibid.,* **129**, 813 (2000).
7. Ziolek M., Sobczak I., Nowak I., Decyk P., Lewandowska A. and Kujawa J., *Microporous and Mesoporous Mat*., **35-36**, 195 (2000).
8. Ziolek M., Sobczak I., Nowak I., Decyk P. and Stoch J.**,** *Stud. Surf. Sci. Catal*., **135**, 07O04 (2001).
9. Ziolek M., Sobczak I., Nowak I., Daturi M. and Lavalley J.C., *Topics in Catalysis,* **11**, 343 (2000).
10. Kim J.Y., Yu J.S. and Kevan L., *Molecular Physics*, **95**, 989 (1998).
11. Xu J., Yu J.S., Lee S.J., Kim B.Y. and Kevan L., *J. Phys. Chem. B*, **104**, 1307 (2000).
12. Pöppl A., Newhouse M. and Kevan L., *J. Phys. Chem*., **99**, 10019 (1995).
13. Jia M.J., Lin W.Y., Zhang W.X., Xiao F.S., Pang W.Q. and Wu T.H., *React. Kinet. Catal. Lett*., **67**, 353 (1999).
14. Decyk P., Trejda M., Lewandowska A. and Ziolek M., *Polish J. Environmental Studies*, **10**, 50 (2001).
15. Decyk P., Trejda M., Ziolek M. and Lewandowska A., *Stud. Surf. Sci. Catal*., (2002), in press.
16. Yuan Z.Y., Liu S.Q., Chen T.H., Wang J.Z. and Li H.X., *J. Chem. Soc. Chem. Commun*., 973 (1995).
17. He N.Y., Bao S.L. and Xu Q.H., *Stud. Surf. Sci. Catal*., **105**, 85 (1997).
18. Wingen A., Anastasievic N., Hollnagel A., Werner D. and Schüth F., *J. Catal*., **193**, 248 (2000).
19. Reddy K.M., Moudrakouski J. and Sayari A., *J. Chem. Soc. Chem. Commun*., 1059 (1994).
20. Gontier S. and Tuel A*., Microporous Mater*., **5**, 161 (1995).
21. Ziolek M. and Nowak I., *Zeolites*, **18**, 356 (1997).
22. Zhang L. and Ying J.Y., *AIChEJ*, **43**, 2793 (1997).
23. Ziolek M., Sobczak I., Lewandowska A., Nowak I., Decyk P., Renn M. and Jankowska B., *Catal. Today*, **70**, 169 (2001).
24. Shelef M., *Chem. Rev*., **95**, 209 (1995).

25. Fritz A. and Pitchon V., *Appl. Catal. B, Environmental*, **13**, 1 (1997).
26. Traa Y., Burger B. and Weitkamp J., *Microporous and Mesoporous Mat.*, **30**, 3 (1999).
27. Busca G., Finocchio E., Ramis G. and Ricchiardi G., *Catal. Today*, **32**, 133 (1996).
28. Nowak I., Kilos B., Ziolek M. and Lewandowska A., *ibid*, **78** (2003).
29. Schumacher K., Grün M. and Unger K.K., *Microporous and Mesoporous Mater.*, **27**, 201 (1999).
30. Dessau R.M., *Zeolites*, **10**, 205 (1990).
31. Alcaraz J.J., Arena B.J., Gillespie R.D. and Holmgren J.S., *Catal. Today*, **43**, 89 (1998).
32. Nowak I., Michalska A., Ziolek M. and Wieczorek W., *Polish J. Chem.*, **77**, 591 (2003).
33. Prakash A.M. and Kevan L., *J. Am. Chem. Soc*., **120**, 13 148 (1998).
34. El-Malki El.M., Santen R.A. and Sachtler W.M.H., *J. Phys. Chem. B*, **103**, 4611 (1999).
35. Broclawik E., Datka J., Gil B. and Kozyra P., *PCCP*, **2**, 401 (2000).
36. Guidry T.F. and Price G.L., *J. Catal*., **181**, 16 (1999).
37. Torre-Abreu C., Ribeiro M.F., Henriques C. and Delahay G., *Appl. Catal. B*: *Environmental*, **12,** 249 (1997).
38. Sarkany J., d'Itri J.L. and Sachtler W.M.H., *Catal. Lett.*, **16**, 241 (1992).
39. Yan J.Y., Sachtler W.M.H. and Kung H.H., *Catal. Today*, **33**, 279 (1997).
40. Yan I.Y., Lei G.D., Sachtler W.M.H. and Kung H.H., *J. Catal*., **161**, 43 (1996).
41. Corma A., Navarro M.T. and Perez-Ramirez J., *J. Chem. Soc. Chem. Commun*., 148 (1994).
42. Chen J., Li Q., Xu R. and Xiao F., *Angew. Chem. Int. Ed. Engl*., **34**, 2694 (1995).
43. Tsyganenko A.A., *Russian Journal of Physical Chemistry*, **56**, 1428 (1982); *The surface properties of silica*, A.P. Legrand Ed., Wiley (1998).
44. Khabtou S., Chevreau T. and Lavalley J.C., *Microporous Mater.*, **3**, 133 (1994).
45. Hadjiivanov K., Saussey J., Freysz J.L. and Lavalley J.C., *Catal. Lett*., **52**, 103 (1998).
46. Ivanova E., Hadjiivanov K., Klissurski D., Bevilacqua M., Armaroli T. and Busca G., *Microporous and Mesoporous Mat.*, **46**, 299 (2001).
47. Hadjiivanov K., *Catal. Rev.-Sci. Eng.*, **42**, 71 (2000).